5G Positioning Based on the Wideband Electromagnetic Vector Antenna

Bo Sun[1], Bo Tan[1], Wenbo Wang[1], Mikko Valkama[1], Christophe Morlaas[2] and Elena-Simona Lohan[1]

[1]*Tampere University, Korkeakoulunkatu 7, Kampusareena, 33720 Tampere, Finland*
[2]*École Nationale de l'Aviation Civile, 7 Avenue Edouard Belin, 31400 Toulouse, France*

Abstract

This work proposed a single base station positioning design in 5G networks, which can jointly estimate user equipment (UE) distance (time of arrival, ToA) and direction (angle of arrival, AoA) by utilizing the wideband 5G signal and vector antenna (VA). A statistics-based Expectation-maximization (EM) algorithm and a subspace-spaced algorithm are adopted to estimate the UE position in this work. The simulation results show that the proposed method can accurately estimate UE position by using the uplink sounding reference signals (SRS) in a Line-of-Sight (LoS) scenario where the tapped delay line D (TDL-D) channel model is used to construct delay and attenuation profiles for multiple paths. Also, the impact of the strong reflections on angle estimation and polarization accuracy is studied in the subspace algorithm. This work proves that the VA is able to provide high accuracy 3D UE positioning in 5G networks without the requirement of multiple cells or multiple antennas. However, the performance of the VA antenna is limited by the coarse angle resolution, which needs to be resolved by VA composed antenna array in future works.

1. Introduction

5G networks are considered as the mainstream mobile network in the next decade and have been deployed worldwide for mobile broadband access from 2019 onwards. 5G provides a variety of communications scenarios like evolved mobile broadband (eMBB), massive machine-type communications (mMTC), and ultra-reliable low latency communications (URLLC) [1]. Driven by the vast range of application scenarios, the mobile network is expected to provide the functions transcending traditional radio connectivity access, for example, the accurate positioning, which is an imperative function needed in the vertical applications, namely, vehicle or drone networks and Industrial 4.0, etc.

ICL-GNSS 2021 WiP Proceedings, June 01–03, 2021, Tampere, Finland
bo.sun@tuni.fi (B. Sun); bo.tan@tuni.fi (B. Tan); wenbo.wang@tuni.fi. (W. Wang); mikko.valkama@tuni.fi (M. Valkama); christophe.morlaas@enac.fr (C. Morlaas); elena-simona.lohan@tuni.fi (E. Lohan)
https://fi.linkedin.com/in/bo-sun-0a5130188 (B. Sun); https://www.tuni.fi/en/bo-tan (B. Tan); https://www.tuni.fi/en/wenbo-wang (W. Wang); https://www.tuni.fi/en/mikko-valkama (M. Valkama); http://ema.recherche.enac.fr/permanent-staff-2/christophe-morlaas/ (C. Morlaas); https://www.tuni.fi/en/elena-simona-lohan (E. Lohan)
0000-0002-5803-4778 (B. Sun); 0000-0002-9085-4266 (B. Tan); 0000-0002-4319-4103 (W. Wang); 0000-0003-0361-0800 (M. Valkama); 0000-0003-4533-1711 (C. Morlaas); 0000-0003-1718-6924 (E. Lohan)

The Global Navigation Satellite System (GNSS) based positioning solutions are intensively studied in literature and has been the default option for most the modern mobile devices when location-based service (LBS) is needed. However, the GNSS solutions often suffer from the Urban Caynon effect (multipath propagation, blockage, and interference) in the area with high building density, where the vehicle/drone applications need the positioning support the most. In addition, two meters positioning accuracy and around 10 Hz update rate of the GNSS solution may not conform with the latency and security requirements in these 5G vertical applications. Thus, to use 5G radio signals for positioning together with communications functions is becoming explicit and trendy research genre, with potential to provide high accuracy and frequent update rate for mission-critical applications. In 3GPP Release 16 [2], the multiple-cell and single-cell positioning scenarios have been defined. The multiple-cell scenarios include the round-trip time (RTT) based trilateration method, angle of arrival/departure (AoA/AoD) based trigonometric method, and the time difference of arrival (TDoA). Researches in [3] and [4] provide the extended Kalman filter (EKF) based positioning solutions of ToA estimation and shows the Cramér–Rao lower bound (CRLB) of the positioning accuracy. Maximum likelihood estimator (MLE) based 5G positioning solution, and its ToA estimation CRLB is given in [5]. However, these multi-cell approaches often require the systematic cooperation, which increases the system complexity and deployment cost, for example, the synchronization between the BSs in TDoA solution. Therefore, in this paper, we will focus on solutions of the single-cell (base station) positioning. The single base station positioning solution proposed in[6] uses tensor-based methods to jointly estimate the AoA and delay with 5G millimeter-wave channel.

The critical element to enable the single-cell positioning is to estimate the angle and delay of the signal source simultaneously on the basestation. The requirement can be achieved by using the phased antenna array receiver for wideband signal perception [7, 8]. Uniform linear array (ULA), uniform circular array (UCA), or uniform rectangular array (URA) are often used for this purpose [9, 10]. Receivers equipped with antenna array have the potential to achieve the high angle resolution by increasing the number of array elements (i.e., increasing the physical aperture); also exhibit limitations, for example limited dimensionality (in ULA and UCA), non-identical angle estimation (in ULA and URA), and distortion occurring on the wideband signals. In this paper, we will introduce the VA to overcome the limitations of the array-based approaches. The VA has gained attention for electromagnetic waves angle-of-arrival (AoA) detection since it was firstly introduced by Arye Nehorai and Eytan Paldi in 1994 [11]. According to Arye and Eytan's work [11], the VA has the capability to estimate the source AoA in a sphere space (i.e., 360°of azimuth and 180°of elevation) without knowing the polarization [12]. The VA designed in [12] can achieve the full space source AoA and polarization detection with various wideband source frequencies from $2GHz$ to $6GHz$. This paper proposes a VA-based single-cell 3D UE positioning method for the 5G system by using the uplink reference signal SRS. The following remarks facilitate the proposed scheme: ***i)***. the SRS signal in the 5G uplink is used as carrier for positioning information (delay and angle); ***ii)***. VA enabled time 3D space positioning; ***iii)***. high accurate subspace- and statistical-based joint angle and time delay estimation methods for 5G UE positioning with single BS.

The rest of this paper is organized as follows: Section 2 describes the 5G SRS signal and basics of VA. Signal model and estimation algorithms are introduced in Section 3. In Section 4, we show the simulation results and analysis. Section 5 concludes the paper and proposes future

work.

2. Reference Signal and Vector Antenna Structures

2.1. 5G Sounding Reference Signal (SRS)

The SRS signal is used in the 5G New Radio (NR) systems for detecting uplink (from UE to base station) channel quality. In 3GPP standards TS 38.211 [13], the SRS is derived from the Zadoff-Chu sequence whose entries are allocated to the specific time and frequency slot (physical resource unit, PRU) by obeying a set of the configuration parameters, which are contained in the signaling messages such as radio resource control (RRC) Connection Setup message and RRC Connection Reconfiguration message. Once a Zadoff-Chu sequence is selected, each entry in the sequence will be allocated to PRU in a resource block (RB) according to the parameters set $[\mathbf{l}_0, \mathbf{k}_0, \mathbf{K}_{tc}, \mathbf{nrofSymbols}, \mathbf{m}_{SRS}, \mathbf{C}_{SRS}, \mathbf{B}_{SRS}]$[1]. $\mathbf{l}_0$ and $\mathbf{k}_0$ determine the initial frequency domain subcarrier index and time domain symbol index. Comb parameter $\mathbf{K}_{tc}$ determines the interval (number of subcarriers) between two contiguous SRS resource elements on frequency domain. **nrofSymbols** defines the duration (number of symbols) of the SRS signal. $\mathbf{m}_{SRS}$ is the total number of PRBs that can be used for SRS transmission. The value of $\mathbf{m}_{SRS}$ is selected from Table 6.4.1.4.3-1 in 3GPP TS 38.211 [13] according to the value of transmission bandwidth indicator $\mathbf{B}_{SRS}$ and bandwidth configuration parameter $\mathbf{C}_{SRS}$. The higher layer of network sends the $\mathbf{B}_{SRS}$ and $\mathbf{C}_{SRS}$ in the RRC message. An example of two UEs SRS signal generation are given in Fig.1.

2.2. Electromagnetic Vector Antenna Structure

Generally, the VA is a type of antenna composed of a total of 6 antenna elements. 3 electric and 3 magnetic dipoles which can detect the 3 Electric(e) and 3 Magnetic(h) fields along x, y, z axis in Cartesian coordinates. As shown in Fig. (2), the electric and magnetic elements of VA are identically and orthogonally oriented between each other. Thus, the VA can detect the electromagnetic wave coming from a sphere space where the center is the location of VA.

3. Research methodology

3.1. Wideband ToA Manifold Construction

5G NR (sub-6GHz) utilizes the wideband OFDM signal of up to 100 MHz in the frequency range from 450 MHz to 6 GHz[14]. For an OFDM signal, the same propagation delay introduces linearly increasing phase shifts on with the ascend subcarrier frequency. This phenomenon makes the base station be able to estimate the UE signal propagation delay by measuring the phase shifts on subcarriers. The delay manifold $\mathbf{g}(\tau) \in \mathbb{C}^{1\times N}$ and received frequency domain SRS signal $s(\tau) \in \mathbb{C}^{1\times N}$ can be described in mathematical models as eq. (1) and (2). Supposing the propagation delay of a SRS signal is τ and the first subcarrier of SRS signal is the reference subcarrier with phase shift $e^{-j2\pi f_0 \tau}$. The phase shift on the n_{th} subcarrier is $e^{-j2\pi f_n \tau}$, where

[1]To avoid the misunderstanding, the symbols $\mathbf{l}_0, \mathbf{k}_0, \mathbf{K}_{tc}, \mathbf{nrofSymbols}, \mathbf{m}_{SRS}, \mathbf{B}_{SRS}, \mathbf{C}_{SRS}$ are the same as 3GPP TS 38.211 [13]

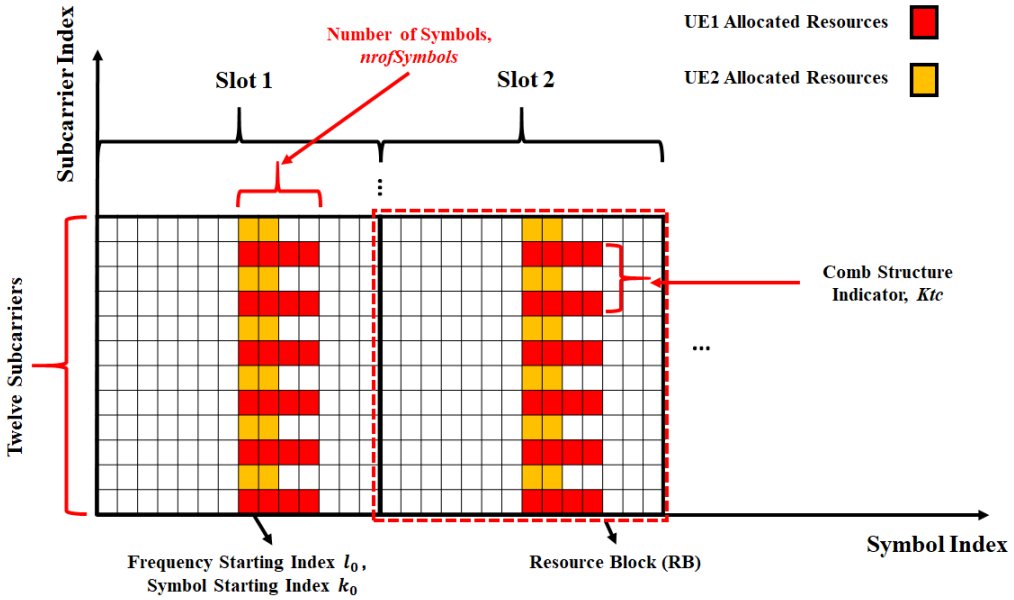

Figure 1: An example of two UEs' SRS signals frequency domain resource allocation pattern. Two resource blocks are exhibited in this example. SRS signals of both UEs start from the $8th$ OFDM symbol but the duration are 4 and 2 for UE1 and UE2.

f_n is constructed by SRS comb parameter K_{tc} and OFDM subcarrier space Δf; The value is $f_n = nK_{tc}\Delta f$. The $[\cdot]^H$ denotes Hermitian transpose. Then, the received SRS signal $s(\tau)$ is the dot multiplication product of the SRS sequence $\mathbf{s_{SRS}} \in \mathbb{C}^{N\times 1}$ and the delay manifold $\mathbf{g}(\tau)$.

$$\mathbf{g}(\tau) = [1, e^{-2j\pi f_1 \tau}, e^{-2j\pi f_2 \tau}, ..., e^{-2j\pi f_{N-1} \tau}]^H \tag{1}$$

$$\mathbf{s}(\tau) = \mathbf{s_{SRS}} \cdot \mathbf{g}(\tau) \tag{2}$$

Assumption 1: According the 3GPP TS 38.211 [13], the SRS signals of different users are allocated into orthogonal time and frequency slots. Thus, there will be no SRS interference from other users when using it for delay and angle estimation.

3.2. 3-D AoA manifold construction

Fig. 3 illustrates the Cartesian system contains one VA and UE. The impinging signal is on direction $\mathbf{u}$, to the base station equipped with the VA. The azimuth and elevation angles of receiving signal are ϕ and θ, respectively. The polarization state of the incoming electromagnetic wave are represented by horizontal and vertical polarization vectors $\mathbf{v}_1^{'}$ and $\mathbf{v}_2^{'}$. By comparing with the reference polarization state vector $\mathbf{v}_1$ and $\mathbf{v}_2$, the auxiliary polarization angle γ can be measured. The polarization phase difference ζ among $\mathbf{v}_1^{'}$ and $\mathbf{v}_2^{'}$ indicates the linear or elliptical polarization state of the EM wave.

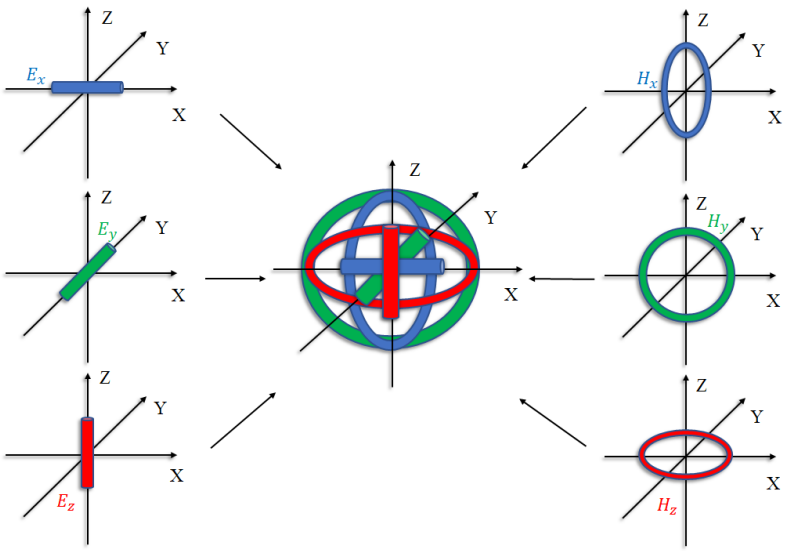

Figure 2: Electromagnetic Vector Antenna Structure, Electrical Dipoles (left), Magnetic Dipole (right)

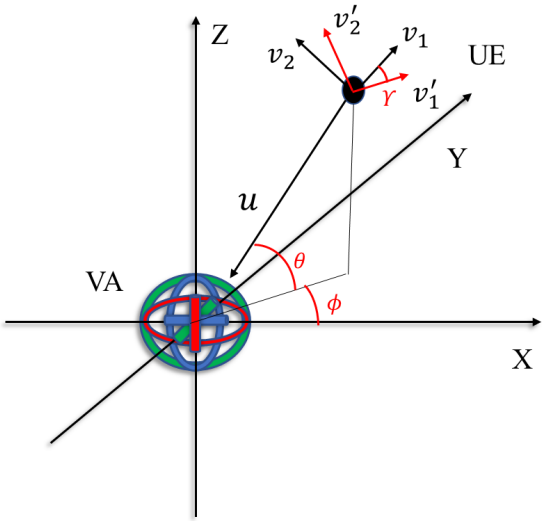

Figure 3: 3D vector antenna Cartesian and orthogonal triad ($\mathbf{n}$, $\mathbf{v}_1$,$\mathbf{v}_2$)

Assumption 2: In the practical scenario, the range between UEs and the base station is more prominent than the antenna near field region and antenna dimensions. The VA is consequently can be treated as a point-like structure and the received electromagnetic wave is a planar wave. Thus, the steering vector used for AoA estimation can be written in the form of eq. (3).

$$\mathbf{d}(\phi,\theta,\gamma,\zeta)=\begin{bmatrix}\mathbf{e}_x\\ \mathbf{e}_y\\ \mathbf{e}_z\\ \mathbf{h}_x\\ \mathbf{h}_y\\ \mathbf{h}_z\end{bmatrix}=\begin{bmatrix}\cos\phi\cos\theta & -\sin\phi\\ \sin\phi\cos\theta & \cos\phi\\ -\sin\theta & 0\\ -\sin\phi & -\cos\phi\cos\theta\\ \cos\phi & -\sin\phi\cos\theta\\ 0 & \sin\theta\end{bmatrix}\begin{bmatrix}\sin\gamma\mathbf{e}^{\mathbf{j}\zeta}\\ \cos\gamma\end{bmatrix} \tag{3}$$

Assumption 3: The polarization phase difference ζ is set as 90° in this work, as the electromagnetic wave received from UEs are mostly linear polarized [15].

3.3. Signal Model for 3-D Positioning

In the practical environment, the SRS symbols received by the base station from the mth UE are usually affected by multipath propagation. Assume the N length raw SRS signal $\mathbf{s}^{\mathbf{m}}_{\mathbf{SRS}} \in \mathbb{C}^{N\times 1}$ goes through K multipaths and each path has different delay and angle that can be represented by the delay manifold $\mathbf{g}^{\mathbf{m}}(\tau_k^m)$ and angle steering vector $\mathbf{d}^{\mathbf{m}}(\theta_k^m,\phi_k^m,\gamma_k^m)$, respectively. Thus, the received frequency-domain signal $\mathbf{Y}^{\mathbf{m}}(\mathbf{t}) \in \mathbb{C}^{6N\times 1}$ of mth UE can be expressed by the eq. (4a) and the noise $\mathbf{N}^{\mathbf{m}} \in \mathbb{C}^{6N\times 1}$ is the Gaussian white additive noise (AWGN). $\mathbf{A}^{\mathbf{m}}_{\mathbf{k}}(\theta_k^m,\phi_k^m,\gamma_k^m,\tau_k^m) \in \mathbb{C}^{6N\times 1}$ in (4b) is the joint time-angle steering vector of 3D estimation. $\mathbf{H}$ and $\otimes$ are conjugate transpose and Kronecker multiplication. To match the six elements of steering vector $\mathbf{d}^{\mathbf{m}}(\theta_k^m,\phi_k^m,\gamma_k^m)$, the SRS signal are correspondingly expended into the form of eq. (4c). It should be noted that, AoA steering vector $\mathbf{d}^{\mathbf{m}}(\theta_k^m,\phi_k^m,\gamma_k^m)$ is set with ζ equals to 90° as the assumption 3 described.

$$\mathbf{Y}^{\mathbf{m}}(\mathbf{t})=\sum_{k=0}^{K}\mathbf{A}^{\mathbf{m}}_{\mathbf{k}}(\theta_k^m,\phi_k^m,\gamma_k^m,\tau_k^m)\cdot\mathbf{s}^{\mathbf{m}}_{\mathbf{k}}+\mathbf{N}^{\mathbf{m}}(\mathbf{t}) \tag{4a}$$

$$\mathbf{A}^{\mathbf{m}}_{\mathbf{k}}(\theta_k^m,\phi_k^m,\gamma_k^m,\tau_k^m)=\mathbf{d}^{\mathbf{m}}(\theta_k^m,\phi_k^m,\gamma_k^m)\otimes\mathbf{g}^{\mathbf{m}}(\tau_k^m) \tag{4b}$$

$$\mathbf{s}^{\mathbf{m}}_{\mathbf{k}}=[1,1,1,1,1,1]\otimes\mathbf{s}^{\mathbf{m}}_{\mathbf{SRS}} \tag{4c}$$

3.4. Estimation algorithms

The two estimation algorithms used in this work are: i) subspace-based signal classification and ii) an Expectation and Maximization (EM) algorithm.

3.4.1. Subspace-Based Approach

The first approach is based on the subspace algorithm Multiple Signal Classification (MUSIC) [8]. The searching space of this work $\mathbf{A}^{\mathbf{m}}_{\mathbf{k}}(\phi_k^m,\theta_k^m,\gamma_k^m,\tau_k^m)$ includes four parameters azimuth, elevation, polarization angles and time delay. To performance the 4-D estimation, we first calculate the auto-correlation matrix:

$$R_{\mathbf{YY}}=\mathbb{E}[\mathbf{Y}^{\mathbf{m}}(\mathbf{t})\mathbf{Y}^{\mathbf{m}}(\mathbf{t})^{*}] \tag{5}$$

where $\mathbb{E}[\cdot]$ denotes expectation, $[\cdot]^*$ means the conjugate transpose. After applying eigenvalue decomposition, we will have $\boldsymbol{\lambda}=[\lambda_1,\lambda_2,...,\lambda_{6N}]$ (with ascending order) and eigen vector $\mathbf{E}_{\mathbf{n}}=$

$[e_1, e_2, ...e_{6N}]$. Then, we can define the noise subspace as:

$$\mathbf{E_n} = [e_1, e_2, ...e_{6N-(K+1)}] \tag{6}$$

K is the number of multipath propagation paths we want to estimate. As the we are focusing on the LoS scenario and the processed SRS signal of different UEs are orthogonal in the time-frequency domains, the estimation of multi UEs' position propblem can be symplified into single-target positioning as long as we extract the SRS signal according to the allocation pattern. Thus, K is set to 1 in the simulation. Then, with the noise subspace, the 4-D spectrum of UE m can be defined as:

$$\mathbf{P}(\phi_k^m, \theta_k^m, \gamma_k^m, \tau_k^m) = \frac{\mathbf{A_k^{*m}}(\phi_k^m, \theta_k^m, \gamma_k^m, \tau_k^m)\mathbf{A_k^m}(\phi_k^m, \theta_k^m, \gamma_k^m, \tau_k^m)}{\mathbf{A_k^{m*}}(\phi_k^m, \theta_k^m, \gamma_k^m, \tau_k^m)\mathbf{E_n}\mathbf{E_n}^*\mathbf{A_k^m}(\phi_k^m, \theta_k^m, \gamma_k^m, \tau_k^m)} \tag{7}$$

After exhaust searching in ϕ, θ, γ and τ dimensions with defined searching steps (ϕ_{step}, θ_{step}, γ_{step} and τ_{step}). The searching steps are chosen according to the trade-off between accuracy requirement and computational complexity. The peak value of $\mathbf{P}(\phi_k^m, \theta_k^m, \gamma_k^m, \tau_k^m)$ determines the estimated signal source position and its polarization state.

3.4.2. Statistics-Based Approach

The EM method follows the space-alternating generalized expectation-maximization (SAGE) design in [7]. This method iteratively uses Expectation step (E-step) and Maximization step (M-step) to update expected signal until the variance between the received signal and expected signal reach the convergence point. The received SRS signal of mth UE is $\mathbf{Y^m(t)}$. It contains K multipath components and kth component $\mathbf{\hat{Y}_k^m}(\tau_k^m)$ is described in eq. (8b). The multipath component includes the received signal $\mathbf{^m}_k$ and noise $\beta_k\mathbf{N_k^m}$. The value of β_k is positive and $\sum_{k=1}^{K}\beta_k = 1$ holds to ensure the noise coming from K paths are equal to the total received noise $\mathbf{N^m}$ defined in eq. (4a). The steering vector and delay manifold of k_{th} path are $\mathbf{d_k^m}(\phi_k^m, \theta_k^m, \gamma_k^m)$ and $\mathbf{g_k^m}(\tau_k^m)$.

$$\mathbf{Y^m(t)} = \sum_{k=0}^{K}\mathbf{\hat{Y}_k^m}(\tau_k^m) \tag{8a}$$

$$\mathbf{\hat{Y}_k^m}(\tau_k^m) = \mathbf{L_k^m}(\tau_k^m) + \beta_k\mathbf{N_k^m}(\tau_k^m) \tag{8b}$$

$$\mathbf{L_k^m}(\tau_k^m) = \mathbf{d_k^m}(\theta_k^m, \phi_k^m, \gamma_k^m)\times(\mathbf{s_{SRS}^m}\cdot\mathbf{g_k^m}(\tau_k^m)) \tag{8c}$$

In the M-step the updated value of $\mathbf{L_k^m}(\tau_k^m)$ can be obtained:

$$\hat{\eta}'(\mathbf{\hat{Y}_k^m}(\tau_k^m)) = \arg\max_{[\phi_k^m, \theta_k^m, \gamma_k^m, \tau_k^m]}\int_0^T \mathbf{d}^*(\phi, \theta, \gamma)\hat{Y}_k^m(\tau_k^m)\mathbf{g}^*(t - \tau_k^m)dt \tag{9}$$

T is the OFDM signal observing duration to cover sequence length and maximum propagation delay. The E-step and M-step will be iteratively implemented until the algorithm reach the convergence point. The value of intermediate noise $\mathbf{N_k^m}$ is used as the convergence condition. The value of $\mathbf{N_k^m}$ keeps changing in each EM iteration and reaches its extreme limit point when the estimated parameters are approximately fully recovered. The extreme limit point of $\mathbf{N_k^m}$ is reached when the power difference of $\mathbf{N_{k,step(n-1)}^m}$ and $\mathbf{N_{k,step(n)}^m}$ in the continuous two steps is approaching the threshold ϵ. The flow chart of the algorithm is shown in Fig. 4

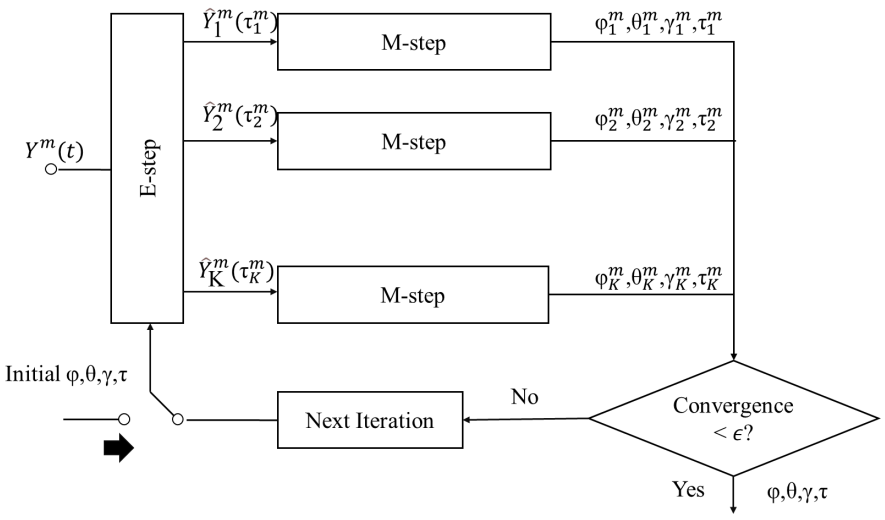

Figure 4: The signal flow of the EM algorithm

4. Simulation Results

4.1. Simulation Setting

Based on the assumptions listed in Section 3, the base station knows the SRS from different UE to perform single target position estimation. In this work, the physical resource allocation pattern of the target UE is the same as the UE1 in Fig.1. In the frequency domain, the total PRB number $\mathbf{m}_{SRS}$ and comb structure indicator $\mathbf{K}_{tc}$ are set to 40 and 2, respectively. The total bandwidth used for SRS is 15MHz as the 15kHz subcarrier spacing is selected. In the time domain, the SRS signal starts from the eighth OFDM symbol and lasts four symbols in every slot. We treat one SRS OFDM symbol as one snapshot in the simulation, and the snapshot number in the estimation is 20, which means the total collected samples last 5 slots.

A LoS communication environment is constructed by using a 3GPP standard TDL-D channel model with 13 taps. The NLoS taps follow the Rayleigh distribution with average attenuation values less than −18dB. The first tap (LoS tap) has a delay of 10ns, which equivalent to 3m radial range. The LoS tap follows a Rice distribution with a K-factor of $K_1 = 13.3$dB and 0dB mean channel attenuation. 10ns is selected for the delay spread of TDL-D channel to simulate the extreme case where multipath propagated signals are arriving with undetectable ToA difference. In addition, we generate AoA profiles for 12 multipath taps, which are not defined in the 3GPP report[16]. The angle step (ϕ_{step}, θ_{step}) and time step (τ_{step}) used in two position estimation methods are 0.4° and 3.3**ns** (1**m**).

4.2. Positioning Performance

This subsection shows the VA-based 3D-positioning performance by using subspace and EM approaches, respectively. We also use the URA as the reference for comparison. Both VA and (3×3) URA-based approaches are capable to detect targets with high accuracy (less than 0.5m

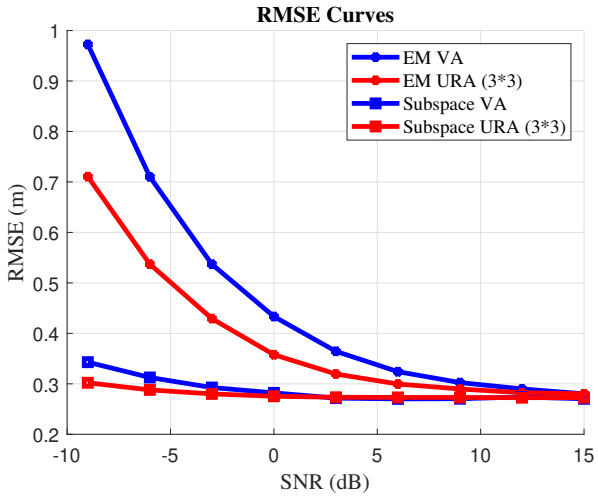

Figure 5: RMSE VS SNR with VA and URA, Source AoA = [30, 30], Source ToA = 10**ns**, TDL-D Channel with 13 Multipaths.

RMSE) even with 0dB SNR. However, EM methods of URA and VA are more sensitive than the subspace-based counterparts with low SNR region. Through comparing VA and URA with the EM method, VA shows lower accuracy than the URA configuration. The performance of both VA and URA approaches gradually converge to 0.3 RMSE when the SNR increases. Thus, we can conclude that the subspace method is more suitable for VA-based positioning systems with the presence of high noise power. It is worth to mentioning that the EM-based method is sensitive to noise power, but it costs less computation time than the subspace-based method. It means the EM approach is a better choice for high SNR to computationally constrained scenarios. We set the target time delay τ_k^m equals to 3.3**ns** in the simulation. But the sector shaped coverage area expands with the increasing radial range (or increasing time delay τ_k^m). Thus, the accuracy of far target will degrade unless we use finer ϕ_{step} and θ_{step} values.We also observe the impact of time searching step (τ_{step}) on RMSE in EM and subspace algorithms. As shown in Fig.6, the larger (τ_{step}) causes the larger RMSE value for both EM- and subspace-based methods; though the larger (τ_{step}) reduces the computation resources consumption in algorithms would, unavoidably, introduces performance degradation. However, the RMSE with 5**ns** time step is 0.4**m** and it is still acceptable for outdoor positioning systems.

4.3. Reflection influence

The signal strength of multipath components of the TDL-D channel is set with values at least 18dB less than the LoS path. To figure out the positioning capability of the proposed work in a strong reflection appeared environment, this subsection explores the reflected signal impact of AoA estimation, Fig.7. shows the results. We assume the VA-equipped station locates in the middle between one wall and one drone; the base station received signal contains one LoS component with 10*ns* time delay (3m) and one reflection from the building has 15*ns* time delay. The AoA of LoS path and reflection are [30, 30] and [120, 120], respectively. To show VA used

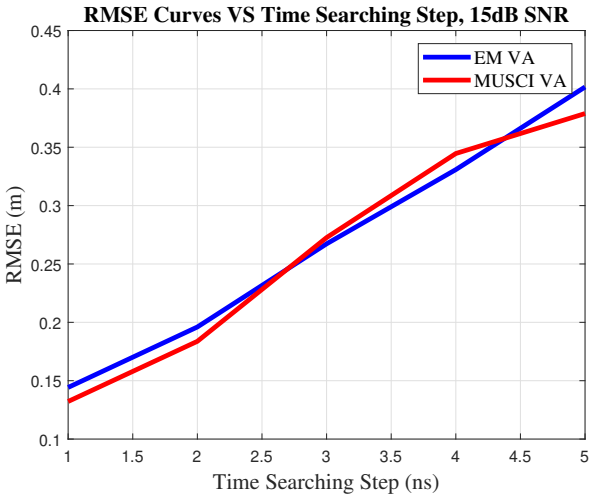

Figure 6: RMSE VS Time Searching Step, Source AoA = [30, 30], Source ToA = 10**ns**, TDL-D Channel with 13 Multipaths, SNR = 15dB.

AoA estimation capability, the Fig.7 plots the subspace spectrum in azimuth and elevation angle dimensions with different reflected signal strengths. When signal power to reflection power ratio (SPRP) equals to 0dB shown in Fig.7.d, the detected target located at a region in the middle between [30, 30] and [120, 120], this means neither the LoS component nor NLoS component can be properly estimated. The detected AoA region is close to [30, 30] when the SPRP is improved to 3dB, but we still cannot correctly figure out the AoA of LoS path. By observing the single LoS path estimation result in the Fig.7.a and weak reflection (10dB SPRP) influenced AoA estimation result in the Fig.7.b; we can find the estimated AoA region are close to the ground truth. In summary, Fig.7 shows AoA estimation with VA is vulnerable in face of multipath influence. Strong multipath path introduces the AoA estimation errors unless the SPRP is higher than 10dB.

4.4. Auxiliary polarization angle impact on positioning performance

The auxiliary polarization angle γ of a UE is usually unknown by the base station in a realistic situation. Thus, the measurement of γ and its relationship with reflections are explored in this section. The setting of source and reflection positions is following subsection 4.3; varying the relative polarization angles γ of the reflection and LoS paths is the new feature discussed in the following content. 4.3.

In Fig.8, we plot the AoA estimation RMSE with the source polarization angle γ ranging from 0 to 2π. The subspace method estimates AoA and polarization angle simultaneously with the presence of only LoS path. The RMSE of AoA stays between 0.3° and 0.4°, which proves that the VA-based design has a stable performance of AoA estimation no matter the signal polarization state is.

According to [11], the polarization angle γ provides one degree of freedom to resolve two impinging electromagnetic waves from the same location. Thus, we assume the signal comes

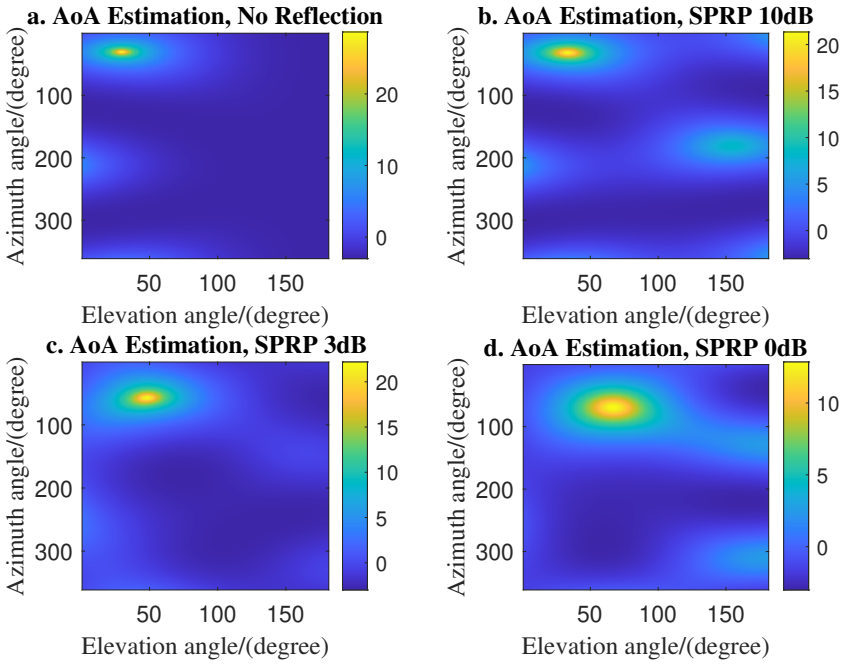

Figure 7: VA-based AoA Estimation with/ without Reflections, Source AoA = [30, 30], Reflection Signal AoA = [120 120], Subspace Method, Signal Power to Reflection Power Ratio = [10dB, 3dB, 0dB]

from a drone that has a fixed 10° polarization angle γ_{LOS} of LoS component and turning reflection γ_{NLOS} from 0 to 2π to check if polarization angle difference between two signals can mitigate strong reflection impact occurs in subsection 4.3.

Fig.9.a shows that the RMSE of AoA estimation various with the different reflection polarization angles. Two RMSE minimum appear when γ_{NLOS} equals to 170° and 340°. To monitor the relationship between the estimated source polarization angle and RMSE curves, the estimated LoS path polarization angle corresponding to the RMSE figure is plot in Fig.9.b. From the estimated polarization angle plot, we can see that the reflection also brings the error into the γ_{LoS} estimation. The curve of estimated γ_{LoS} reach its minimum when γ_{NLOS} has values close to 180° and 350°. Surprisingly, the minimum point of AoA RMSE curve and the correct γ_{LoS} value (10°), have strong connections; the AoA RMSE value reduces if the γ_{NLOS} and γ_{LoS} have about π or 2π difference. However, Fig. 9 shows the AoA estimation error still is exists with the absence of coherent signal from different paths even with orthogonal γ values (γ_{NLOS} = 100°).

5. Conclusion

This paper proposes a VA based 3D positioning method with EM- and subspace-based algorithms under the 5G-NR network. The positioning function achieved using up-link dedicated reference signal SRS, and the LoS scenario is constructed with TDL-D channel model. The simulation results have shown that both subspace- and EM-based methods can estimate the target position

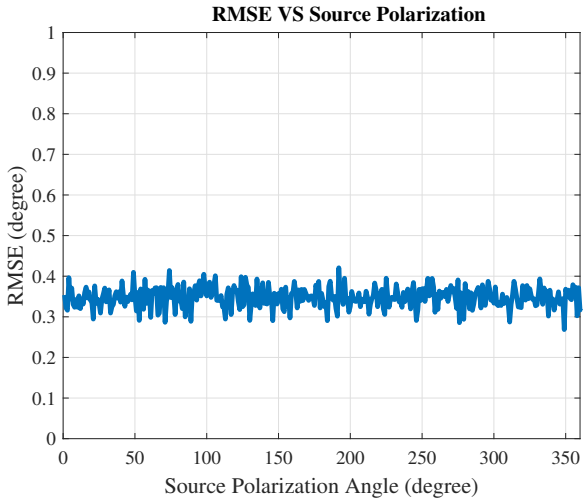

Figure 8: VA-based AoA Estimation with reflections, Source AoA = [30, 30], Without Reflection, Subspace Method

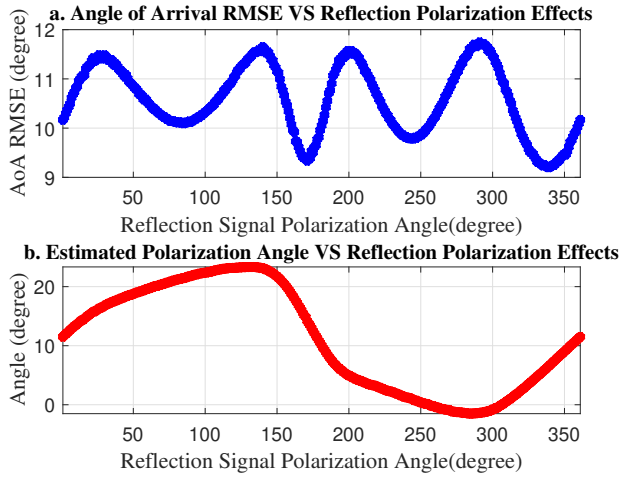

Figure 9: VA-based AoA Estimation with reflections, Source AoA = [30, 30], Reflection Signal AoA = [120 120], SPRP Ratio = 8dB ,Subspace Method

accurately with either VA or URA; the subspace method provides better performance with low SNR values, and EM costs less computation resource. Subspace method significantly improves the VA's performance with low SNR region. Although VA has slightly worse performance than URA with the two estimation algorithms, it has an outstanding broader coverage than URA, which is only capable of source detecting in a hemisphere area. We believe VA based 5G positioning system can perform a reliable, accurate, and robust performance in a 3D space. In practice, the proper time step selection is necessary to balance the limitations of computation resources and desired accuracy. Moreover, the presence of a strong multipath reflection causes the AoA estimation performance deterioration. The reflection influence can somehow be eased

if the multipath component auxiliary polarization angle has π difference in comparison with the LoS polarization angle. Since the communication environment is not controllable and the adjustment of auxiliary polarization angle is almost impossible in real life. Our future work will focus on the VA array constructed 5G positioning systems to improve the positioning accuracy with the presence of strong reflections.

Acknowledgments

This research was partly funded by the SESAR Joint Undertaking (SJU) in project NewSense (Evaluation of 5G Network and mmWave Radar Sensors to Enhance Surveillance of the Airport Surface), Grant Number 893917, within the framework of the European Union's Horizon 2020 research and innovation program. The opinions expressed herein re□ect the authors' view only. Under no circumstances shall the SJU be responsible for any use that may be made of the information contained herein. This work was also partly supported by the Academy of Finland, under the project ULTRA (328226, 328214).

References

[1] M. Fallgran, M. Dillinger, Z. Li, G. Vivier, T. Abbas, J. Alonso-Zarate, T. Mahmoodi, S. Alli, T. Svensson, G. Fodor, On Selected V2X Technology Components and Enablers from the 5GCAR Project, IEEE International Symposium on Broadband Multimedia Systems and Broadcasting, BMSB 2018-June (2018) 3–7. doi:10.1109/BMSB.2018.8436731.

[2] 3GPP, TS 138 211 - V16.3.0 - 5G; NR; Physical channels and modulation (3GPP TS 38.211 version 16.3.0 Release 16) 0 (2020).

[3] E. Y. Menta, N. Malm, R. Jantti, K. Ruttik, M. Costa, K. Leppanen, On the Performance of AoA-Based Localization in 5G Ultra-Dense Networks, IEEE Access 7 (2019) 33870–33880. doi:10.1109/ACCESS.2019.2903633.

[4] Y. Lu, M. Koivisto, J. Talvitie, M. Valkama, E. S. Lohan, Ekf-based and geometry-based positioning under location uncertainty of access nodes in indoor environment, in: 2019 International Conference on Indoor Positioning and Indoor Navigation (IPIN), 2019, pp. 1–7. doi:10.1109/IPIN.2019.8911785.

[5] J. Huang, J. Liang, S. Luo, Method and Analysis of TOA-Based Localization in 5G Ultra-Dense Networks with Randomly Distributed Nodes, IEEE Access 7 (2019) 174986–175002. doi:10.1109/ACCESS.2019.2957380.

[6] F. Wen, H. Wymeersch, 5G Synchronization, Positioning, and Mapping from Diffuse Multipath, IEEE Wireless Communications Letters 10 (2021) 43–47. doi:10.1109/LWC.2020.3020116.

[7] J. Fessler, A. Hero, Space-alternating generalized expectation-maximization algorithm, IEEE Transactions on Signal Processing 42 (1994) 2664–2677. doi:10.1109/78.324732.

[8] R. O. Schmidt, Multiple emitter location and signal parameter estimation, Adaptive Antennas for Wireless Communications 34 (1986) 276–280. doi:10.1109/9780470544075.ch2.

[9] B. Sun, B. Tan, W. Wang, E. S. Lohan, A comparative study of 3d ue positioning in 5g new

radio with a single station, Sensors 21 (2021). URL: https://www.mdpi.com/1424-8220/21/4/1178. doi:10.3390/s21041178.

[10] B. Tan, K. Chetty, K. Jamieson, ThruMapper: Through-wall building tomography with a single mapping robot, HotMobile 2017 - Proceedings of the 18th International Workshop on Mobile Computing Systems and Applications (2017) 1–6. doi:10.1145/3032970.3032973.

[11] A. Nehorai, E. Paldi, Vector - Sensor Array Processing for, IEEE Transactions on signal processing 42 (1994).

[12] J. Duplouy, C. Morlaas, H. Aubert, P. Potier, P. Pouliguen, C. Djoma, Wideband and reconfigurable vector antenna using radiation pattern diversity for 3-d direction-of-arrival estimation, IEEE Transactions on Antennas and Propagation 67 (2019) 3586–3596. doi:10.1109/TAP.2019.2905729.

[13] 3GPP, 5G;NR;Physical channels and modulation, Technical Specification (TS) 38.211, 3rd Generation Partnership Project (3GPP), 2018. URL: https://portal.3gpp.org/desktopmodules/Specifications/SpecificationDetails.aspx?specificationId=3213, version 15.2.0.

[14] 3GPP, NR;User Equipment (UE) radio transmission and reception;Part 1: Range 1 Standalone, Technical Specification (TS) 38.101.1, 3rd Generation Partnership Project (3GPP), 2021. URL: https://www.3gpp.org/ftp//Specs/archive/38_series/38.101-1/, version 17.0.0.

[15] R.Meenakshi, G.Premalatha, Circularly polarized monopole mobile phone antenna for gnss applications, International Research Journal of Engineering and Technology (IRJET) 03 (2016) 757–760.

[16] Study on Channel Model for Frequency Spectrum Above 6 GHz, Technical Report, 2016. URL: https://www.etsi.org/deliver/etsi_tr/138900_138999/138900/14.02.00_60/tr_138900v140200p.pdf, v14.0.0.